



This is a repository copy of *Laser-induced breakdown spectroscopy measurements of mean mixture fraction in turbulent methane flames with a novel calibration scheme*.

White Rose Research Online URL for this paper:
<https://eprints.whiterose.ac.uk/175315/>

Version: Published Version

Article:

Kotzagianni, M. orcid.org/0000-0002-4834-6196, Yuan, R., Mastorakos, E. et al. (1 more author) (2016) Laser-induced breakdown spectroscopy measurements of mean mixture fraction in turbulent methane flames with a novel calibration scheme. *Combustion and Flame*, 167. pp. 72-85. ISSN 0010-2180

<https://doi.org/10.1016/j.combustflame.2016.02.025>

Reuse

This article is distributed under the terms of the Creative Commons Attribution (CC BY) licence. This licence allows you to distribute, remix, tweak, and build upon the work, even commercially, as long as you credit the authors for the original work. More information and the full terms of the licence here:
<https://creativecommons.org/licenses/>

Takedown

If you consider content in White Rose Research Online to be in breach of UK law, please notify us by emailing eprints@whiterose.ac.uk including the URL of the record and the reason for the withdrawal request.



eprints@whiterose.ac.uk
<https://eprints.whiterose.ac.uk/>



Laser-induced breakdown spectroscopy measurements of mean mixture fraction in turbulent methane flames with a novel calibration scheme



M. Kotzagianni^{a,b,*}, R. Yuan^a, E. Mastorakos^a, S. Couris^b

^a Hopkinson Laboratory, Engineering Department, University of Cambridge, Cambridge CB2 1PZ, UK

^b Physics Department, University of Patras, Patras, 26504, Greece and Institute of Chemical Engineering Sciences, Foundation for Research and Technology–Hellas (ICE-HT/FORTH), Patras, 26504, Greece

ARTICLE INFO

Article history:

Received 30 September 2014

Revised 22 February 2016

Accepted 23 February 2016

Available online 16 March 2016

Keywords:

Laser Induced Breakdown Spectroscopy

(LIBS)

Calibration

Mixture fraction

Swirling flame

Turbulent flame

Non-premixed flame

ABSTRACT

Laser Induced Breakdown Spectroscopy (LIBS) was applied to homogenous methane–air mixtures of a wide range of compositions ranging from only air to only fuel in order to establish a new calibration scheme suitable for LIBS measurement of mixture fraction in turbulent non-premixed flames. Both a portable low resolution spectrometer equipped with a CCD detector with wide temporal detection window and a monochromator with a fast gated ICCD camera were employed to monitor the plasma emission. The results obtained using the two detection systems were fully consistent, suggesting that LIBS can be used successfully with the CCD detector that is more suitable for industrial applications. From the spectroscopic analysis, it was shown that the ratio of the intensities of H_{α} (656.3 nm) over O (777.3 nm) (H_{α}/O) and of C_2 ($\Delta v=0$, $d^3\Pi_g - \#x03B1;^3\Pi_u$) over CN ($\Delta v=0$, $B^2\Sigma^+ - X^2\Sigma^+$) (C_2/CN) depend monotonically on the mole fraction of methane in the ranges of 0.0–0.3 and 0.3–1.0 respectively, therefore providing a new scheme for measurement of mixture fraction in non-premixed systems spanning the complete range of equivalence ratios. The technique was also applied to a swirling recirculating premixed flame and it was found that the equivalence ratio is successfully measured in both reactants and products. Based on the above, LIBS experiments were then carried out in turbulent axisymmetric non-reacting and reacting jets, and the mean mixture fraction determined by the aforementioned calibration curves was in good agreement with empirical correlations, while the rms measurement showed the expected trends, demonstrating hence the usefulness of the technique.

© 2016 The Authors. Published by Elsevier Inc. on behalf of The Combustion Institute.

This is an open access article under the CC BY license (<http://creativecommons.org/licenses/by/4.0/>).

1. Introduction

During the past few years, Laser Induced Breakdown Spectroscopy (LIBS), a laser-based spectroscopic or analytical technique, has been developed and successfully applied for combustion diagnostics purposes [1–3]. By strongly focusing the beam of a laser system in the flame region, dissociation of the present molecules and/or ionization is occurring forming the plasma. After the collection and monitoring of the plasma-emitted radiation and its spectroscopic analysis, one can retrieve information about the fuel content (and/or the Air-to-Fuel Ratio) of various combustible mixtures and infer the local chemical composition [4], determine

parameters of the flame such as the temperature [5], and/or identify the fuel used [6]. After the first application of LIBS in hydrocarbon–air mixture by Schmieder [7], a large number of studies have been presented in various combustion systems under different conditions. In the majority of the previous LIBS works, the ratio of some spectral lines of atomic origin like the ratio H_{α}/O (at 777 nm) [4,6,8–15] or O/H_{α} [16], the ratio H_{α}/N (at 567 nm or 744 nm) [17–19] or sometimes both [20–22], are employed most of the times for the determination of the equivalence ratio and rarely for the determination of the concentration (in %) of a constituent. Sometimes emission lines attributed to carbon atoms are also used since these emission lines are directly linked to the fuel. Thus, either the ratio of a carbon line to a nitrogen, hydrogen or oxygen line like C/H_{α} and C/N (at 500.5 nm) [5], the ratio C (at 833 nm)/ N (at 744 nm) with C (at 833 nm)/ O (at 777 nm) [23], or C (at 711.3 nm)/ O (at 776.6 nm) and C (711.3 nm)/ N (at 746.3 and 743.8 nm) [24], or the ratio of the intensity of a carbon line

* Corresponding author at: Hopkinson Laboratory, Engineering Department, University of Cambridge, Cambridge CB2 1PZ, UK.

E-mail address: mk760@cam.ac.uk, m.kotzagianni@lav.mavt.ethz.ch (M. Kotzagianni).

to the sum of intensities of a nitrogen and an oxygen line C (at 711 nm)/[N (at 744 nm)+O 777-nm] [24] have been successfully used. However, there are limited calibration curves based on the ratio of a molecular band to atomic lines like CN (integrated from 705 to 733 nm)/N (at 746.3 nm or 743.8 nm), or CN (integrated from 705 to 733 nm)/O (at 776.6 nm) or CN (integrated from 705 to 733 nm)/[N (at 744 nm)+O (at 777 nm)] [25], or based on the intensity of molecular bands like CN ($\Delta v=1, 0, -1, B^2\Sigma^+ - X^2\Sigma^+$) [26], CN ($\Delta v=0, B^2\Sigma^+ - X^2\Sigma^+$) [27,28].

Most of the work above concerned lean mixtures. To expand LIBS to fully non-premixed systems, Do et al. [29] have employed the ratio H_α/N (at 568 nm) and the N/H_α for the determination of the fuel concentration in methane- and ethylene-air mixtures with fuel mole fractions up to 90%. The analysis and the fuel measurement were retrieved from emission spectra which have been obtained with a detection window of 20 ns duration using an ICCD camera. From a more practical point of view, such a delicate detection system would be a rather limiting factor for the LIBS application under very aggressive industrial conditions. In addition, this work has not explored in detail the application of the technique and the calibration scheme to turbulent non-premixed flames.

Concerning the precision of the single shot results, which is necessary for instantaneous mixture fraction (or equivalence ratio) measurements in turbulent non-premixed systems, some investigations have demonstrated [24,25] that the equivalence ratio calculated from the instantaneous measurements is accurate even if there is some dispersion of the values of the equivalence ratio greater in fuel-rich in comparison to the fuel-lean mixtures. However, there is no extensive study on the precision of LIBS for turbulent systems.

Finally, it is important to note that in turbulent combustion one must be able to measure in both reactants and products. In fully premixed flames, the carbon to oxygen atomic ratio does not change across the flame (once any small-scale differential diffusion effects have been smoothed out), but the species composition and temperature are very different. The decrease in density and the large amounts of CO_2 in the hot products suggest that a higher energy is needed to produce a spark, and the presence or not of a spark has been exploited to actually establish the boundary of the flame brush [10,30]. However, if the laser energy is high enough, one may expect that a spark will always be created in both reactants and products and hence a measurement of the same equivalence ratio across a premixed flame would suggest that LIBS can measure the mixture fraction in combusting systems irrespective of the degree of reaction, which is a necessary requirement for the measurement of mixture fraction in non-premixed flames.

Examination of the aforementioned literature suggests that no molecular line other than the one of cyanogen band has been employed as an indicator of the amount of fuel in the mixture so far, and that up to now, the technique has been applied only to a small range of compositions. However, when non-premixed turbulent combustion systems are under investigation, with the corresponding severe changes of fuel concentrations both locally and temporally, further work is needed (i) to develop calibration strategies spanning a wider range of mixtures than before; (ii) to ensure plasma creation in both the low- and high-temperature regions; and (iii) to investigate the precision of single-shot results.

This paper explores the application of LIBS technique for local and instantaneous measurements of the equivalence ratio in turbulent premixed and non-premixed flames. The key novelty lies in the use of the technique for highly turbulent systems and for a much wider range of equivalence ratio than before using a new calibration strategy. In the remaining of this paper, we describe the LIBS measurements using two different detection systems as applied in uniform mixtures spanning a very wide range of compositions so as to create calibration curves, which are then used

for the study of turbulent premixed and non-premixed flames. The paper closes with a summary of the most important conclusions.

2. Experimental methods

2.1. Flow conditions

For the needs of the present research, initially homogeneous flowing methane/air mixtures, exiting from a $d = 23$ mm inner diameter (ID) tube, were used (burner (I) in Fig. 1). The flow rates of the mixture varied from 10 SLPM to 200 SLPM, which corresponds to velocities of 0.4–8.0 m/s, and therefore Reynolds numbers of 586–11720. Based on the fact that the mixtures were fully mixed and uniformly distributed across the pipe, in the immediate exit of the pipe (i.e. at low height to diameter (h/d) values; $h/d < 0.4$), the acquired results were used as calibration curves for the subsequent investigation. In order to characterize the methane-air mixtures of different compositions, the mole fraction of methane, X_{CH_4} , was in the range from 0 to 1.

Following the calibration, turbulent flames were investigated. For non-premixed flames, the burner (II) (Fig. 1) consisted of two coaxial stainless steel tubes; a mixture of 70% methane and 30% air by volume (equivalence ratio 22.21) was supplied from the inner tube of 5 mm ID and with the length-to-diameter ratio 128, while laminar airflow was coming out from the outer tube of 200 mm ID to surround and protect the mixture and/or the flame from disturbances from the environment [31]. The jet exit velocity of the mixture was 17 m/s and the velocity of the surrounding air was 0.1 m/s. In some experiments, the CH_4 volume fraction was 30%, which is too low for a jet turbulent flame to stabilize and therefore the measurement of the fuel at the spark location corresponds to a measurement of an inert tracer.

For premixed systems, a recirculating methane-air flame, which resulted from the bluff-body burner (III) (Fig. 1) developed by Cavaliere et al. [32] but adjusted to the framework of the present investigation, namely without the enclosure, was studied. In this configuration, the CH_4 -air mixture was supplied from a pipe of length 350 mm and ID 37 mm, which in the center contained a conical bluff-body (45° half-angle) with diameter 25 mm. A swirler produced an azimuthal velocity component, which reinforced the recirculation zone in the wake of the bluff body and caused a widening of the flame. Note that the flame is exposed to the ambient air, so it is expected the equivalence ratio to drop to zero at large distances from the flame brush; however, to remain the same in the reactants and the products across the flame. For these experiments, the equivalence ratio was 0.81 and the bulk velocity at the annulus was 10.2 m/s.

In all cases the reactants, namely the methane and the air, were supplied by a high purity bottle (99.99%) and an air compressor respectively, while their flow rates were regulated and measured by calibrated rotameters. The air compressor was equipped with a drier and with moisture and oil filters, which resulted in dry air being delivered. This is important because even small amounts of moisture in the atmospheric air can contribute to the hydrogen line in the LIBS spectra. However such contribution in the intensity of hydrogen line arising from the humidity present in the air was taken into account and subtracted in any case from the rest of the results shown.

2.2. LIBS experimental setup and data acquisition

Two sets of experiments were performed. The first set was with uniform mixtures and was aimed at establishing the suitability of calibration schemes and the importance of the detection system and the laser energy. The second set was with the turbulent

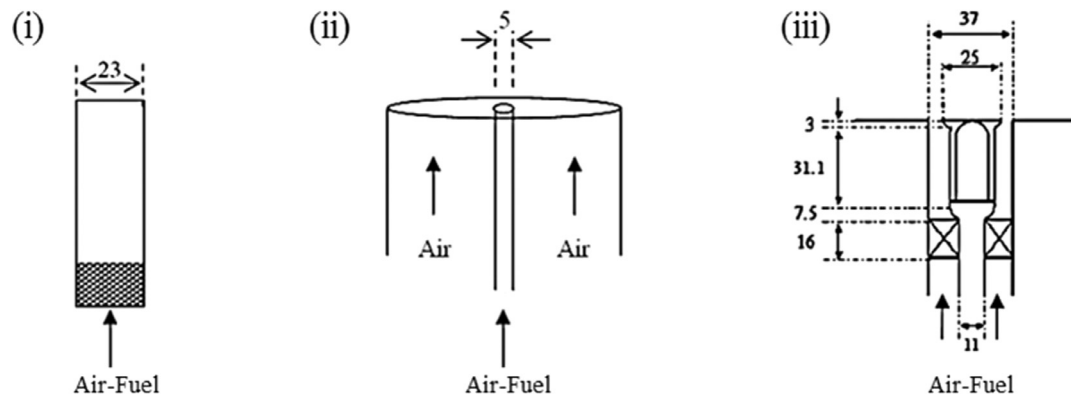


Fig. 1. Schematic of the experimental arrangements used for calibration (I), turbulent jet non-premixed flames (II) and turbulent premixed flames (III). All dimensions in mm.

flames. Note that whenever the laser, optics, or acquisition parameters change, a new calibration curve with identical settings should be created to make LIBS quantitative, so the turbulent flame studies should always be preceded by a calibration exercise with the same system.

2.2.1. 1st Experimental setup

For the experiments carried out in order to assess the impact of the detection system on the plasma emission spectra, the laser employed was a 4 ns Nd:YAG laser (EKSPLA NT342) operating at 1064 nm at a repetition rate of 10 Hz. The laser beam was focused by means of a 50 mm focal length plano-convex lens, 2 mm above and on the centerline of the Bunsen burner. The light emitted from the induced plasma was collected using a 25.4 mm focal length plano-convex lens and via an optical fiber it was fed into one of the two following detection systems. The first one was a 0.46 m monochromator (HR 460, Jobin-Yvon) carrying a turret with two interchangeable optical gratings of 150 and 600 lines/mm, adjustable entrance slit and having attached a 512×512 ICCD camera (Intensified Charge Coupled Device-Andor iStar). The slit was selected to be $50 \mu\text{m}$ and the 150 lines/mm optical grating was employed during the present investigation covering an optical window of 173 nm range. The ICCD camera was externally triggered by the output electrical signal of the laser and the temporal parameters of detection were chosen to be 1.28 μs for the time delay, i.e. the total time elapsed between plasma formation and the measurement, while the acquisition time, i.e. the time width was either 4 μs or 3 ms. The long time was chosen to coincide with the integration time of the non-gated detector so that the performance of the latter can be assessed. In order to detect the spectral lines of interest, two different detection windows were used. The first one covered a 365 to 540 nm spectral region, where the CN 388.3 nm and the C_2 516.5 nm molecular bands were apparent, while the optical area of the second spectrum was extending from 620 to 800 nm for the acquisition of the H_α 656.3 nm and the O 777.3 nm atomic lines. The detection windows were chosen in that way for the purpose of recording the spectral features defining each ratio in the same measurement simultaneously, increasing by this means the accuracy of the results. The second acquisition detector was a 0.075 m portable spectrometer with fixed entrance slit at $50 \mu\text{m}$ holding a 2048 pixel CCD detector (AvaSpec-2048-USB2-UA). The spectrometer was equipped with a 300 lines/mm optical grating and it covered a spectral region from 180 to 1100 nm with one single measurement. The detection window had 3 ms time duration, while the inserted delay time was 1.28 μs . The energy of the laser beam, measured using a pyro electric energy meter, was set to be 40 mJ.

2.2.2. 2nd experimental setup

Finally, a new set of calibration curves together with the experiments on the turbulent lifted jet and turbulent swirling premixed methane-air flame were performed using the focused beam of a Q-switched Nd:YAG laser (Continuum Surelite) delivering 6 ns pulses, operating at 1064 nm and at a repetition rate of 10 Hz. The beam was focused 8 mm above and in the center of the 23 mm-diameter burner, where the mixture was uniform, so as to develop the new necessary calibration curves obtained under the same experimental conditions as the rest of the presented results. In order to ensure breakdown in every position within the flame, the laser energy was set at 250 mJ. The laser beam was focused using a 150 mm focal length plano-convex lens and the plasma was observed to be induced at the same location along the beam path every time. In order to investigate the effect of the laser energy, the laser energy was set also to be 155 mJ and 300 mJ. Note that the employed laser energy is generally considered high, but this is necessary to ensure consistent plasma creation in the hot combustion products. The plasma emission was collected by a 100 mm-focal length lens to an optical fiber attached to a portable spectrometer (Ocean Optics USB 2000). The spectrometer had $50 \mu\text{m}$ entrance slit and it was equipped with a 600 line/mm optical grating, and a CCD detector covering a wavelength range of 178–877 nm. The minimum integration time of the signal on the CCD detector was 3 ms, while the time delay (t_d) was 8 μs , which corresponded to the minimum response time to the triggering signal of the detector.

The plasma emissions were processed in two different ways. In the first case, called “averaging method”, each spectrum was the average of 100 spectra accumulated through the spectrometer’s software (i.e. based on at least 100 sparks at the same position). In the alternative way, here called “instantaneous method”, 100 different single shot spectra, acquired at the same position, were analyzed to give 100 instantaneous measurements of the emission spectra. Examinations of the results from the instantaneous method in the uniform mixtures used for calibration also results in an assessment of the precision of the technique. Finally, the spark was imaged with a camera (Photron Fastcam SA1.1-8 GB memory). The probe volume was found to have approximately length in the long dimension of 3.2 mm and width 0.2 mm, which gave a volume of 0.359 mm^3 with RMS to be 0.01 mm^3 , for plasma induced in ambient air by a Q-switched Nd:YAG laser (1064 nm, 6 ns, 10 Hz) with energy $E_{laser} = 155 \text{ mJ}$ focused by a plano-convex lens with focal length of 150 mm. Due to the larger ionization potential of gases containing CO_2 compared to air, we expect that sparking in hot products produces a smaller probe volume than the one in air. The laser beam was traversed across the flame

in the radial direction and normal to the beam's path, so that the expected steep gradients in the radial direction are better resolved.

3. Results and discussion

In this section, the emission spectra of the plasma induced in uniform flows of air, of methane, and of mixtures of air–methane of various compositions are first described and compared to each other. The intensities of all spectral features of interest are correlated to the mole fraction of methane of each mixture. The LIBS technique is then applied to recirculating premixed flame giving information about the equivalence ratio distribution both in the products and the reactants area. Finally, the mapping of the mean mixture fraction in a lifted turbulent jet flame and a non-reacting jet is demonstrated and the results are compared successfully to empirical expressions.

3.1. Uniform methane–air mixtures: calibration curves

3.1.1. General behavior

The impact of the amount of fuel of premixed homogenous methane–air mixtures of various compositions on the LIBS spectra was investigated and the results are shown in Fig. 2. The LIBS spectra in the air and in pure methane are also shown in the same figure. The results exhibited were acquired using the two detection systems, the CCD (Fig. 2.I) and the ICCD (Fig. 2.II) under the same temporal parameters ($t_d = 1.28 \mu\text{s}$ and $t_w = 3 \text{ms}$), while the employed laser energy was 40 mJ. The detectable optical range of the spectra recorded with the CCD and the ICCD camera were 920 nm and 173 nm; however in Fig. 2, the spectra acquired from the CCD camera are zoomed in around the region of interest; namely 300–900 nm.

From Fig. 2a, which corresponds to plasma induced in air ($X_{\text{CH}_4} = 0$), it can be seen that the emission spectrum is basically dominated by atomic lines of oxygen and nitrogen. Some of the most intense ones are the N(I)-744.2 nm, N(I)-821.6 nm, N(I)-871.1 nm and O(I)-777.3 nm, O(I)-844.6 nm whereas most of them are triplets with the more familiar examples to be the N(I)-744.2 nm and O(I)-777.3 nm consisting of the N(I)742.4, 744.2, 746.8 nm lines and the O(I) 777.2, 777.4 and 777.5 nm lines respectively [33]. All these emissions originate from the dissociation of the nitrogen and oxygen molecules present in the dry air that was used, while no emissions related to carbon-containing molecules or carbon atoms are apparent, as expected.

In the case of mixing of the dry air with fuel and especially at $X_{\text{CH}_4} = 0.1$ ($\varphi = 1$) as shown in Fig. 2b, some additional emissions are observed in the spectra. In more detail, apart from the emissions correlated with the molecules of air, the molecular bands of cyanogen are also clearly observed. The CN emission consists of the vibrational sequences $\Delta v = 1, 0, -1$ of the CN band system $\text{B}^2\Sigma^+ - \text{X}^2\Sigma^+$ and are observed around 359.0 nm, 388.3 nm and 421.6 nm respectively. The origin of these molecules is stemming from the dissociation of carbon- (CH_4) and nitrogen containing molecules in the plasma, which then combine leading to the formation of energetically excited molecules of CN [34,35]. Apart from the CN molecular bands, the atomic lines of hydrogen, namely the H_α at 656.3 nm and the H_β at 486.1 nm, are also intensely depicted in the spectra, while their presence is also attributed to the dissociation of the methane molecules and can be used as an indicator of the fuel.

When LIBS is performed in very rich mixtures, as for example at mixtures with $X_{\text{CH}_4} = 0.75$ ($\varphi = 28.56$) depicted in Fig. 2c, some new molecular bands are dominating the spectra. These spectral features are exhibited at the visible region of the spectra and especially at 473.7, 516.5 and 563.5 nm and they are assigned to the

C_2 Swan system $d^3\Pi_g - a^3\Pi_u$ with $\Delta v = 1, 0, -1$. Moreover, it is also noteworthy to point out the absence of the atomic lines associated to the molecules of nitrogen and oxygen and the substantial decrease of the intensity of the hydrogen lines and of cyanogen molecular bands. Finally, some further LIBS experiments were carried out in pure fuel ($X_{\text{CH}_4} = 1$). From Fig. 2d, it is apparent that almost all of the aforementioned emissions are absent except for the emissions assigned to the C_2 Swan band and the H_α , both of which originate from the dissociation and atomization of the only species present (methane).

To conclude, in the typical LIBS spectra shown in Fig. 2, one can observe that none of the aforementioned spectral lines are present under all fuel mass fractions. Thus, the CN molecular band is clearly observed only in Fig. 2b and c, since the presence of both nitrogen and methane is required for the CN molecule formation, while the absence of one of these two constituents results in the absence of the CN band from the acquired spectra. Moreover, the H_α atomic line is clearly observable in the emission spectra (b), (c) and (d). In contrast, the C_2 molecular band and the oxygen line exhibit a more complicated behavior. Their appearance in the spectra is not only dependent on the presence or not of the corresponding molecules, namely CH_4 and O_2 , but also on their concentration in the mixture. So in the case of a stoichiometric flame, the C_2 molecular band is absent from the emission spectrum and the oxygen line is clearly observable, whereas in the case of a very rich methane–air mixture, the intensity of the C_2 band is significantly enhanced and the O 777.3 nm is thoroughly attenuated. The fact that diverse spectral features are shown in the methane–air mixtures of different compositions means that the composition of the mixture and especially the concentration of fuel in the mixture affect strongly the plasma emission spectra, fostering some new molecules to form, i.e. the C_2 , whereas other characteristic spectral features extensively reported in hydrocarbon–air LIBS experiments [4,6,8–15] to completely extinguish from the emission spectra.

3.1.2. Calibration scheme

The emission spectra monitored by the two detectors corresponding to the same mixture seem to be analogous, while no background emission attributed to Bremsstrahlung radiation is detected in any of the spectra. As a result, it is obvious that a direct quantitative analysis based on the total intensities of the most important and intense spectral lines, namely H_α -656.3 nm, O-777.3 nm, CN-388.3 nm, and C_2 -516.5 nm, is allowed. So as to further explore the dependence between the intensity of these spectral features present in the different spectra to the amount of fuel in the mixture, a systematic sequence of LIBS experiments was carried out in air–methane mixtures of fuel mole fraction ranging from $X_{\text{CH}_4} = 0-1$ ($\varphi = 0-\infty$). Each spectrum is the average of 100 scans accumulated by the ICCD and the CCD cameras having taken into account any noise as e.g. room lighting etc. Also, each data point corresponds to the integrated area below the emission line, while the ratios introduced in the next are determined using the averaging method.

Figure 3a, b, d and e shows the total intensities of the atomic lines H_α -656.3 nm and O-777.3 nm and of the molecular bands of the CN-388.3 nm and C_2 -516.5 nm respectively, obtained by the ICCD and the CCD detector, as a function of the mole fraction of methane in the various mixtures. The laser energy was 40 mJ and the time delay and time width were the same as before (1.28 μs and 3 ms, respectively). From Fig. 3a and b, one can distinguish clearly a different behavior between the hydrogen and the oxygen lines. The O-777.3 nm emission is decreasing monotonically and sharply with the mole fraction, while it is completely attenuated at $X_{\text{CH}_4} = 0.23$ for the CCD detection and $X_{\text{CH}_4} = 0.61$ for the ICCD detection. The overall declining behavior of the intensity of the oxygen line can be attributed partly to the ongoing reduction

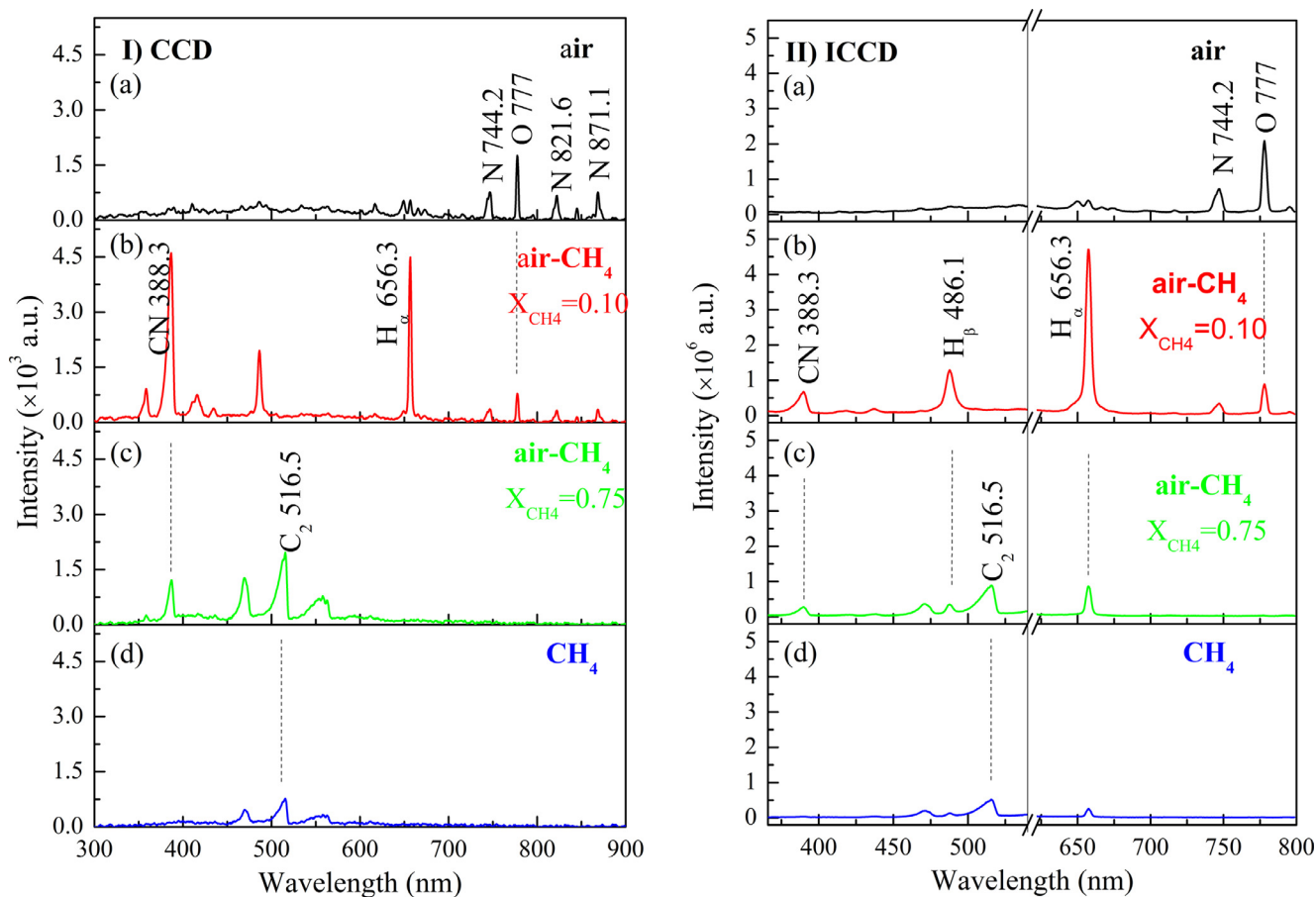


Fig. 2. Emission spectra of laser induced plasma in methane-air mixtures with (a) $X_{\text{CH}_4} = 0$, (b) $X_{\text{CH}_4} = 0.10$, (c) $X_{\text{CH}_4} = 0.75$, and (d) $X_{\text{CH}_4} = 1$ acquired with a CCD (left) and an ICCD (right) detection system. The laser energy was set at 40 mJ and the time delay and time width were 1.28 μs and 3 ms, respectively.

of the concentration of the oxygen molecules in the mixture resulting both in the dissociation of less molecules and partly to a diminished total intensity, or to the acquisition times of the detector. In the second case, according to Ferioli et al. [24], a shorter delay time is recommended since there is a strong impact on the measured lifetimes of the emission lines as a function of the concentration of fuel and the quenching effects stemming from high rate cooling of the plasma, rapidly changing species concentrations.

In contrast, the hydrogen line, after an almost linear increase reached a plateau and then decayed until $X_{\text{CH}_4} = 0.5$ for the CCD detection and $X_{\text{CH}_4} = 0.65$ for the ICCD detection, where the emission of the atomic line could not be distinguished from the background emission. Perhaps the expected behavior of the H_α line would be the ongoing built-up of its intensity as the amount of fuel increases in the mixture for all X_{CH_4} . However, such a behavior is not observed, while from the trend of the data points of the H_α emission, it seems possible that self-absorption effects might have occurred during the experiments. Furthermore, the rapid decay of the hydrogen line for $X_{\text{CH}_4} > 0.2$, despite the abundance of hydrogen atoms originating from the methane in such mixtures, could alternatively imply some radical-removal chemical mechanism since the rapid decay of the hydrogen line and the disappearance of the oxygen line approximately coincide to the initiation of the formation of the C_2 molecular band, as it will be discussed later. During their experimental research on hydrocarbon liquid-gas mixtures, Kido et al. [36] reported that in rich and high pressure environments the quenching of hydrogen emission is expected to be stronger, which is in accordance to the experimental findings of the current work.

Figure 3d shows that the CN band emission is increasing almost linearly with the mole fraction of methane in the range of 0.0–0.10 for both detection systems. This behavior has been reported in the past when optical breakdown was induced either by electrical spark or by ns/fs laser pulses in methane–air mixtures [26–28]. For even higher values of mole fraction of methane, the emission of the CN band flattens out for $0.10 < X_{\text{CH}_4} < 0.3$ and eventually decreases to zero. This is probably attributed to the fact that any further increase of the amount of fuel in the mixture means also a simultaneous lack of nitrogen molecules, which has as a result the ensuing decrease of the intensity of CN band. However, such a decrease in the CN intensity occurring at fuel rich mixtures has also been reported in the past by Sturm et al. [37]. During their study, the authors investigated unreactive mixtures of $\text{C}_3\text{H}_8\text{--N}_2$ in the absence of O_2 and therefore flame. According to these authors, this behavior could be due to the fact that the environment of the plasma formation might influence the results since both the absorption and the plasma conditions may change from case to case and especially when only fuel is present.

The intensity of the C_2 molecular band appears to be practically zero for values of mole fraction of methane lower than 0.2, and then a sudden increase of its intensity is observed until $X_{\text{CH}_4} = 0.5$ for the CCD detection and $X_{\text{CH}_4} = 0.65$ for the ICCD detection. After reaching a plateau, the intensity of the C_2 band decreases to a small, but finite value at $X_{\text{CH}_4} = 1$. Based on this, one could conclude that the formation of the C_2 molecules is a direct consequence of the excess of fuel, while it also affects the trend of the CN band intensity, which is attenuated due to the consumption of carbon atoms for the C_2 molecule formation. Finally, the decaying trend of the emission of the C_2 and of other intermediates could

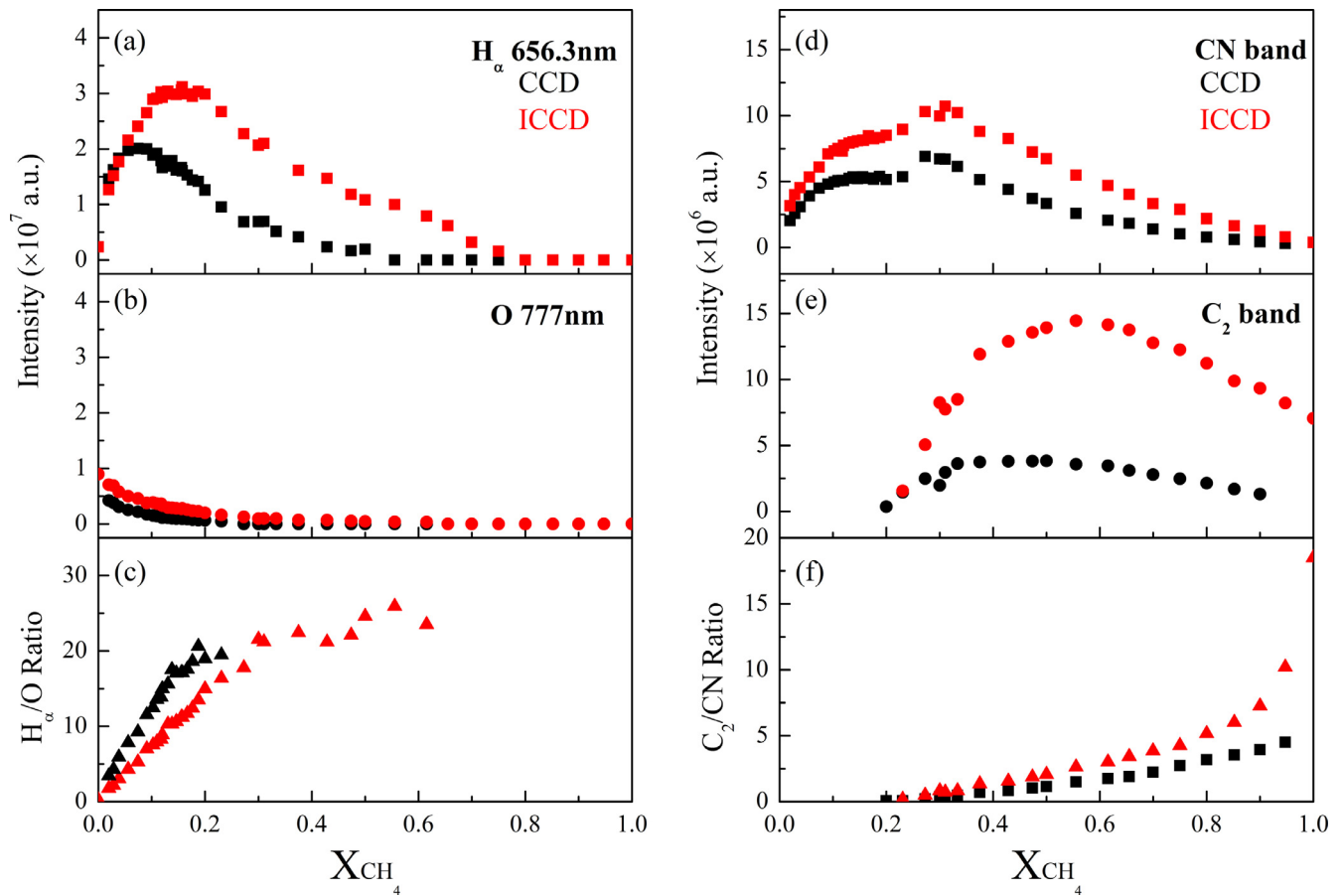


Fig. 3. Total intensity of (a) H_{α} and (b) O (777.3 nm) atomic lines and of (d) CN (388 nm) and (e) C_2 (516.5 nm) molecular bands together with the corresponding ratios, (c) H_{α}/O and (f) C_2/CN , calculated by the averaging method, versus the X_{CH_4} calculated from LIBS spectra acquired using the ICCD (red symbols) and the CCD (black symbols) detector.

be related to the presence of the combustion products like water and CO_2 far from the spark which could cause the decrease of the observed intensities as it is reported by Li et al. [38] who employed a similar spectroscopic technique (femtosecond filament excitation) in ethanol/air flame stabilized on an alcohol burner.

Although the physical mechanisms leading to the reduction of some emissions with increasing methane content are not fully understood yet, a correlation of the H_{α}/O and C_2/CN versus the mole fraction of methane in the mixture is obtained. The ratios are essentially independent of various experimental parameters, such as the collection system and the fluctuations of the laser energy, or stochastic events, like the plasma formation. This renders them reliable for direct correlation to the actual mole fraction of methane. Figure 3c and f shows the H_{α}/O and C_2/CN ratio as a function of the mole fraction of methane, in mixtures of various compositions, derived from the spectra recorded by the two detection systems. Each data point was obtained by the averaging method. In the case of molecular emissions, the total intensity was determined by the total intensity of the corresponding head bands.

In Fig. 3c and f, one can clearly observe that both ratios span in a monotonic way the increase of the mole fraction of methane. In more detail, the ratio H_{α}/O exhibits a linear dependence on the amount of fuel up to values $X_{CH_4} = 0.18$ for CCD detection and up to $X_{CH_4} = 0.30$ for ICCD detection, while the ratio C_2/CN reveal an also monotonic dependence on the X_{CH_4} commencing from $X_{CH_4} = 0.3$. As a result of all these considerations, one could suggest that the calibration curves of the Fig. 3c and f could be applied for the estimation of the methane content. The x-axis can alternatively be expressed in terms of the mass fraction of

methane, which can be inferred as the mixture fraction in flames, or in terms of the equivalence ratio. Out of all the spectral features in the acquired emission spectrum, the C_2 molecular band is the clearest indicator of which of the two ratios should be used. So, in the case of absence of the C_2 molecular band, the H_{α}/O ratio (Fig. 3c) will be the right diagnostic tool for the determination of the X_{CH_4} , while the presence of the C_2 band implies that the C_2/CN ratio (Fig. 3f) should be used. This measurement strategy will be employed for turbulent combustion flames with large fluctuations in equivalence ratio in Sections 3.3 and 3.4 and is suggested as a novel LIBS method for non-premixed combustion systems.

3.1.3. Effect of detector type

In addition to the above analysis, which is of both qualitative (emission spectra of Fig. 2) and quantitative (intensity dependence on X_{CH_4} and corresponding calibration curves of Fig. 3) nature, some remarks regarding the efficiency of the detection systems are given here. In the past, either a CCD [4,8–10,13,18,19,22, etc.] or an ICCD [6,11,12,16,17,21,23, etc.] detector has been employed for the detection of the plasma emission in LIBS, and one report [39] discusses the usage of two ICCD cameras for the planar detection of the whole plasma using band-pass filters. Although there are some comparative studies regarding the performance of CCD and ICCD detectors in solid samples like brass [40,41] aluminum and lead-tin alloy block [40], sintered iron oxide containing silicon or aluminum [42], steel [43], geologic materials [44] and in objects of cultural heritage [45], there has been no such comparison for combustible systems. Hence, from Figs. 2 and 3, it is easily observed that the overall trends of both the spectral lines and the ratios as a function

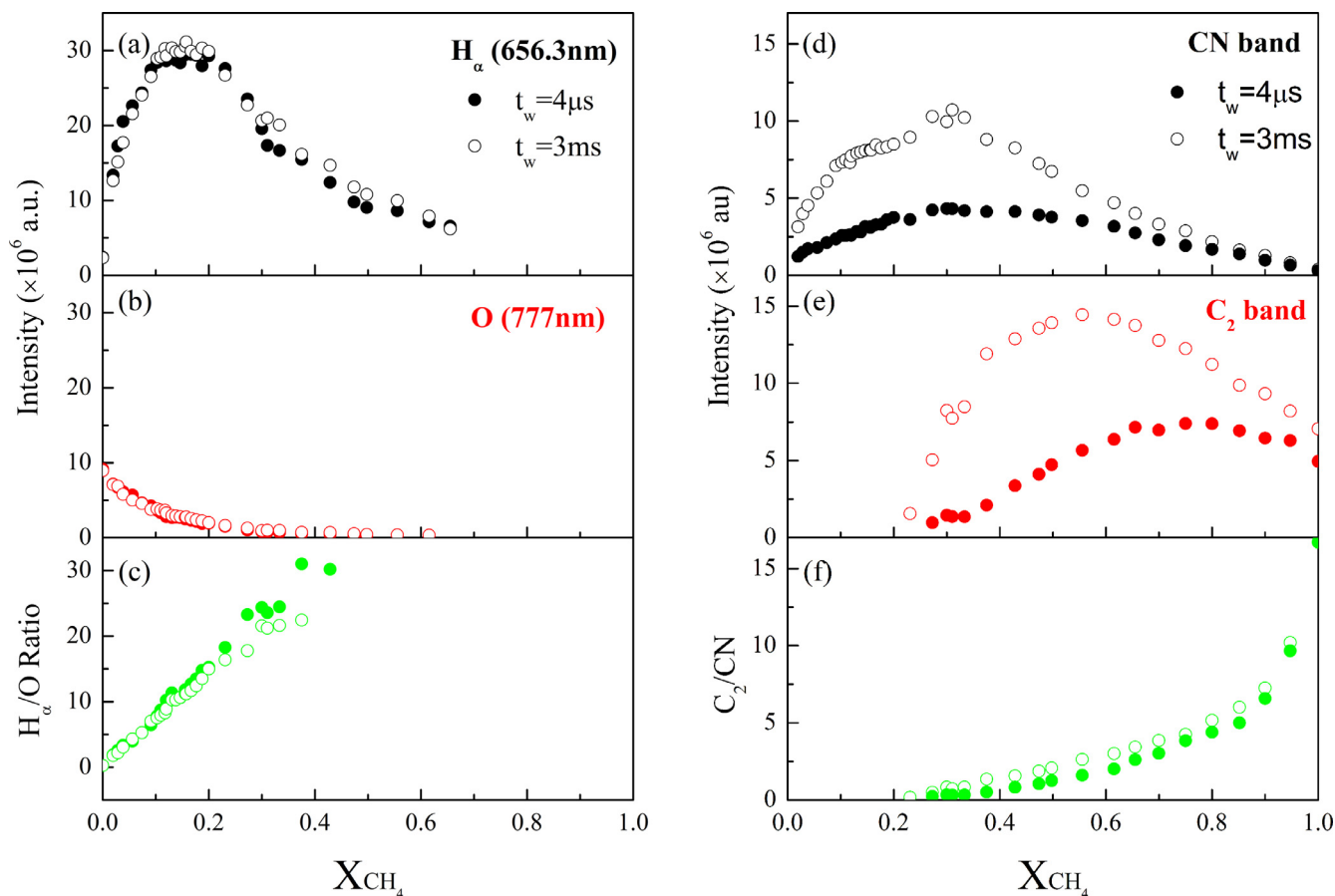


Fig. 4. Total intensity of (a) H_{α} and (b) O (777.3 nm) atomic lines and of (d) CN (388 nm) and (e) C_2 (516.5 nm) molecular bands together with the ratios, (c) H_{α}/O and (f) C_2/CN calculated by the averaging method versus the X_{CH_4} calculated from LIBS spectra acquired using the ICCD detector for two different detection windows.

of the mole fraction are almost the same. The difference observed at the intensities of the various lines and the limits of detection of the weakest lines (the H_{α} and O-777.3 nm) are probably attributed to the quantum efficiency of the detectors, without influencing significantly the diagnostic tools that this investigation is focused on.

The fact that the usefulness of the ratios to provide calibration for a wide range of ϕ does not depend on the detector type suggests that time-resolved conditions are not necessarily required to perform the compositional analysis of the flammable mixture, while the advantages arising from size and cost reduction and the portability of the CCD detection system can be used for versatile and rapid analysis of mixtures composition in aggressive environments.

Although the results between the two detectors are the same, the influence of the duration of the light acquisition on the intensity of the various spectral lines monitored by the ICCD camera is important to explore and the results are presented in Fig. 4. Here, the time delay was $1.28 \mu s$ and the integration times were either $4 \mu s$ or 3 ms. The integration time of $4 \mu s$ is a typical value often employed in LIBS experiments, which assures good signal to noise ratio, while the integration time of 3 ms is selected in order to simulate the temporal detection window of the spectrometers equipped with CCD detectors and in particular the Ocean optics spectrometer (3 ms was the minimum detection window it could operate). It is evident that the large detection time (which is what will be employed also in the next set of measurements for the mapping of the turbulent flames) affects only the intensities of the molecular bands of cyanogen and of C_2 , whereas the atomic lines

exhibit the same behavior basically due to their shorter lifetime in comparison to the molecular bands.

In other words, at the end of the detection window of $4 \mu s$, the atomic lines have already, generally, decayed almost totally that they have no other contribution to their total intensity for higher detection times. In contrast, this is not the case for the molecular bands which exhibit significant higher intensities for wider detection windows. So, one could assume that this increase could be linked to the fact that a part of the detected CN emission is associated to the chemiluminescence of the flame which was not detected at such short temporal detection window. As found by collecting light without LIBS spark, the flame luminosity is very low compared to the spark emission. Nevertheless, fuel rich flames could be sooty leading to observable flame luminosity that could potentially be added to the collected emission and subsequently interfere with the intensities of the aforementioned molecular bands (CN and C_2) resulted from the plasma formation. In order to avoid that, the intensity of the luminosity of the flame, even being lower compared to the intensities resulting from the LIBS spectra, was removed at the processing stage when the LIBS spectra are analyzed to evaluate the area under the peaks.

The higher intensities of the molecular bands for longer detection windows could be potentially associated with the longer lifetime of the emission lines in a sense that significant radiation is emitted for longer time after the plasma formation. In Fig. 4, on the one hand, the filled symbols correspond to intensities from radiation emitted during a time interval from $1.28 \mu s$ up to $5.28 \mu s$, while on the other hand, the empty symbols correspond to intensities from a time interval from $1.28 \mu s$ to $3001.28 \mu s$. Based on the

fact that the lifetime of a molecular band is some tens of microseconds, it is expected that significant amount of radiation is collected even after the end of the first detection window ($5.28 \mu\text{s}$) and added to the initial values of intensities (filled symbols) until the end of the second detection window ($3001.28 \mu\text{s}$) and this could probably explain the higher intensities that the molecular bands hold in the latter case. So, since the molecular bands live for much longer, any increase of the detection window up to a point would enhance their intensities. In particular, in the case of C_2 molecular band, its intensity is rising by following a similar trend, whilst in the case of CN molecular band, one can notice that there is a sudden increase of the CN band around $X_{\text{CH}_4} = 0.3$, which was not exhibited in the case of $t_w = 4 \mu\text{s}$. This sudden change observed in the intensity of CN band is not yet understood. It could be associated with chemical reactions that are taking place in the fuel rich mixtures boosting the CN intensity. Also the formation and appearance of the C_2 molecular band in the LIBS spectra may play a role to this sudden increase of the CN intensity, but in any case further investigation is mandatory on the subject. In parallel to these results, the ratios H_α/O and C_2/CN are shown to be entirely independent from the integration time (Fig. 4c and f) exhibiting identical trend for both integration times, establishing the reliability of the CCD detectors for such diagnostic purposes.

3.1.4. Effect of laser energy

Another aspect to be considered is the influence of the energy of the laser beam on the spectral lines intensity (Fig. 5) and on the introduced diagnostic tools (Fig. 6). To perform this investigation, the Ocean Optic CCD spectrometer was used giving identical emission spectra to the ones already presented under the same experimental conditions ($t_d = 8 \mu\text{s}$ and $t_w = 3 \text{ms}$) with the other CCD (AvaSpec-2048-USB2-UA) spectrometer. The laser energy was modified by a combination of a $\lambda/2$ wave-plate with a Glan-Taylor prism polarizer so that beam profile changes due to lamps high voltage and Q-switching parameters are minimized. The employed energies here were $E_{\text{laser},1} = 155 \text{mJ}$, $E_{\text{laser},2} = 230 \text{mJ}$, and $E_{\text{laser},3} = 300 \text{mJ}$. The data from Fig. 5 exhibit the direct impact of the laser energy on the intensity of the atomic and molecular lines, extending the detection range of atomic lines and simultaneously enhancing the intensity of the molecular bands. Thus, in the case of the lowest energy ($E = 155 \text{mJ}$), the H_α and O lines are detectable only for mixtures with mole fraction less than 0.45 and 0.20, respectively, whereas in the case of the highest laser energy ($E = 300 \text{mJ}$) the same lines are still observable at mixtures with $X_{\text{CH}_4} = 0.65$ and $X_{\text{CH}_4} = 0.40$. However, the formation and first appearance of the C_2 band in the spectra is not clearly affected by the high energy of the laser beam, since the C_2 molecular band is detectable at mixtures with the same mole fraction, suggesting that the C_2 molecules are related more to the mole fraction of methane and the chemical reactions taking place in rich mixtures rather than the impact of the laser energy on the plasma formation.

From Fig. 6a, one can notice that for X_{CH_4} in the range of 0.0–0.3, there is an almost linear dependence of the H_α/O ratio to the mole fraction of methane for all values of the laser energy tested. In particular, in the case of the lowest laser energy, represented by the square symbols in the graph, the linearity is valid until $X_{\text{CH}_4} = 0.3$ while as the laser energy increases this linear dependence is extended to higher values of mole fraction. So for $E_{\text{laser}} = 230 \text{mJ}$, close to the energy used during the experiments with the turbulent flames discussed later in this paper, the H_α/O ratio is proportional to the mole fraction up to $X_{\text{CH}_4} = 0.5$, while it reaches a maximum for $X_{\text{CH}_4} = 0.6$ for the highest employed energy ($E_{\text{laser}} = 300 \text{mJ}$). Such progression is mostly caused by the O-777 nm line, because the higher energy gives rise to more excited atoms of oxygen making the lifetime of the atomic line and the chemical history in general shifted to longer times [24]. This means

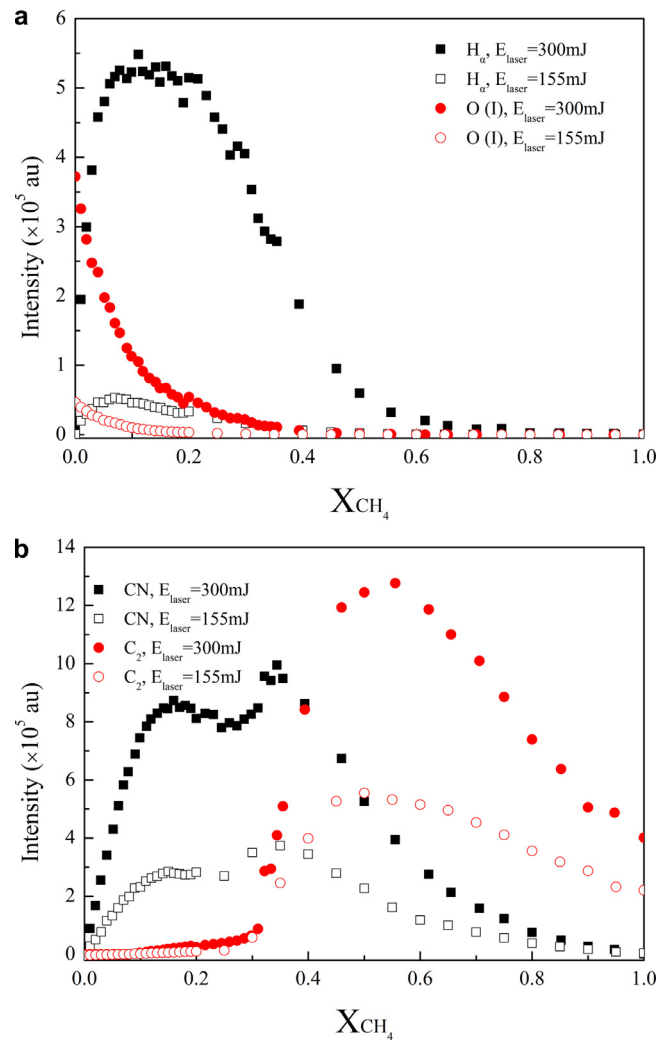


Fig. 5. Total intensity of (a) H_α and O (777.3 nm) atomic lines and of (b) CN (388 nm) and C_2 (516.5 nm) bands, calculated by the averaging method, versus X_{CH_4} for two different laser energies ($E_{\text{laser}} = 155 \text{mJ}$ and $E_{\text{laser}} = 300 \text{mJ}$).

that under the current detector temporal configuration and for the higher energy, the O-777.3 nm line can be detected in even richer mixtures. But even if this linear dependence seems to be enhanced by the increase of the laser energy for $X_{\text{CH}_4} > 0.35$, this ratio could safely be used as a calibration curve in the range $0.0 < X_{\text{CH}_4} < 0.3$ while the rest of the region is out of interest.

In a similar way, Fig. 6b illustrates the C_2/CN ratio, which is zero for values of mole fraction of methane lower than 0.3, in accordance to the comments on Fig. 5. As mentioned already, the C_2 molecular band appears to occur efficiently only at very rich fuel-air mixtures explaining why the ratio is negligible until that value, but after the formation of the C_2 band, the ratio is monotonically increasing to the mole fraction of methane up to $X_{\text{CH}_4} = 0.9$ for all employed laser energies. In the case of even more methane in the mixture, the intensity of the CN molecular band is becoming very weak eventually reaching the intensity of the background emission, suggesting that the ratio blows-up for such extreme values. The laser energy had no actual role in the ratio C_2/CN for values of X_{CH_4} up to 0.9, while the differences observed in the values of the C_2/CN ratio for the different energies and for mole fraction ranging between 0.9 and 1.0 are related to the almost complete absence of the CN band.

It is concluded that although the absolute magnitude of the atomic lines and molecular bands are affected by the laser energy,

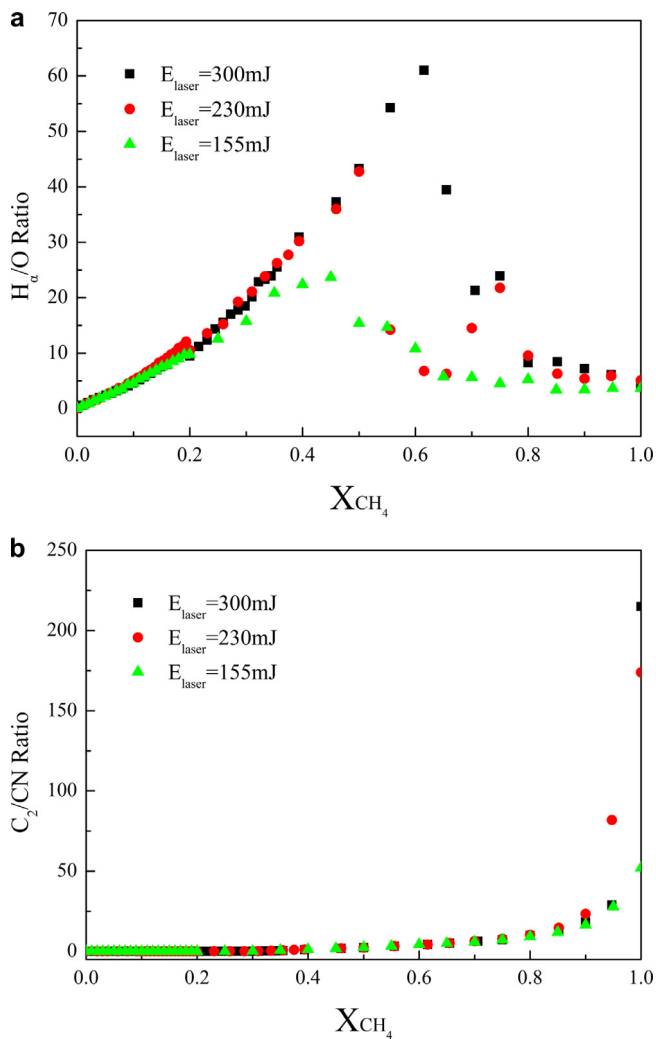


Fig. 6. Calibration curve for the ratio (a) H_{α}/O and (b) C_2/CN as a function of X_{CH_4} , calculated by the averaging method, as measured from LIBS spectra measured at three different laser energies.

the ratios are not affected much and therefore the measurement strategy described before does not depend on the laser energy, although it is preferable to establish calibration curves corresponding to the same or similar energy as during the actual turbulent flame experiments. In the latter case, the LIBS technique is applied to different environments where the discrimination between the reactants and the non-reactants is impossible or in cases where the exact composition of the mixture is unknown, which suggests the absorbed energy may vary from case to case. However, a calibration curve with a special treatment which would include corrections based on the exact composition of the mixture or the distinction between reactants and non-reactants would not be useful under the present investigation. In contrast, there is a clear need for a universal calibration curve performed under similar experimental conditions as the actual measurements in various flames stabilized in more complicated burners.

3.2. Uniform methane–air mixtures: shot-to-shot variation

Measurements in turbulent flames, that may have large temporal and spatial fluctuations in equivalence ratio, necessitate a study of shot-to-shot variations [46]. To assess the precision of the technique, LIBS experiments were carried out in uniform premixed methane–air mixtures and the results, summarized in Figs. 7 and

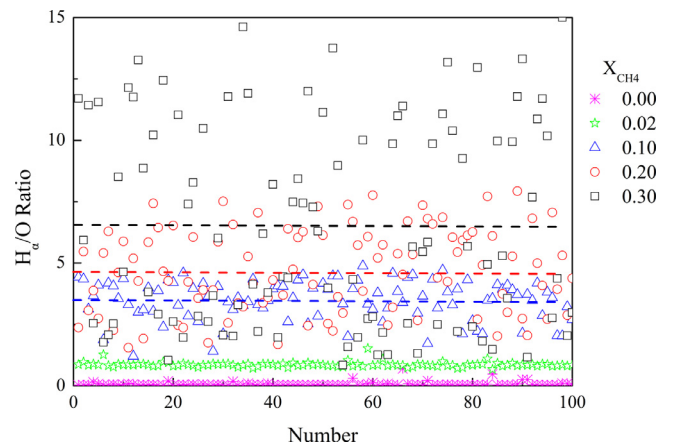


Fig. 7. Ratio H_{α}/O obtained in air and in the indicated mixture of CH_4 -air for 100 single shot spectra. The dashed lines represent the average values of the ratio in the cases of $X_{CH_4} = 0.10, 0.20,$ and 0.30 .

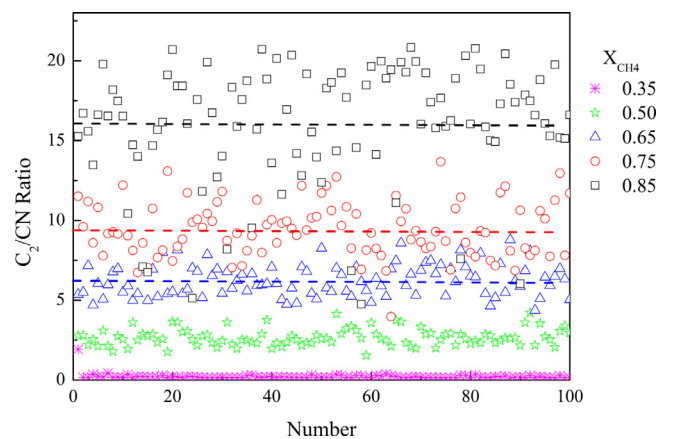


Fig. 8. Ratio C_2/CN obtained in the indicated mixtures of CH_4 -air for 100 single shot spectra. The dashed lines represent the average values of the ratio in the cases of $X_{CH_4} = 0.65, 0.75,$ and 0.85 .

8, were acquired based on the analysis of 100 single-shot independent measurements.

In detail, Figs. 7 and 8 show respectively the single shot line intensity ratio H_{α}/O -777.3 nm and C_2/CN ratio plotted for different mole fractions of methane. Each data point corresponds to a single shot in uniform mixtures having the indicated composition. As can be seen, for $X_{CH_4} < 0.1$, the shot-to-shot standard deviation of the H_{α}/O ratio is small and about 10% of the mean value. As the mole fraction of methane gets higher, these variations increase significantly to about 30% for $X_{CH_4} = 0.2$ and to about 60% for $X_{CH_4} = 0.3$. This behavior is observed at the region of mole fraction where the decay of the H_{α} and O atomic lines was found in Fig. 5. This could potentially suggest that a greater stochasticity of the plasma processes might be associated with the reduction of the intensities of the emission lines and their following detection, leading to a larger divergence from the average value. In contrast, such an increase in the shot-to-shot of the C_2/CN ratios versus X_{CH_4} is not occurring, as can be seen in Fig. 8. The standard deviation of the C_2/CN ratio appears to be equal to 30% of the mean value of $X_{CH_4} = 0.35$, as the C_2 intensity appears to be low at this condition, while for all $X_{CH_4} > 0.35$, the standard deviation of C_2/CN ratio remains roughly at 16–23% of the corresponding mean value. This latter scatter can be affected by a number of different parameters, such as the energy stability of the laser source, the plasma's temperature and electronic density, or even the interaction with the mixture. Similar investigations have been performed in the past by Ferioli et al.

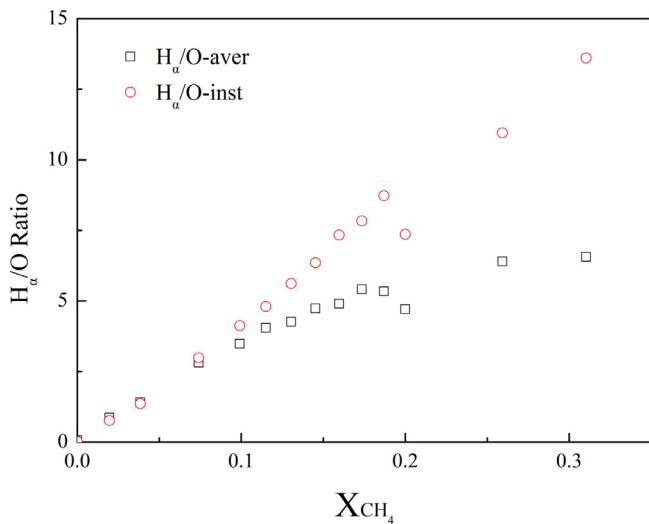


Fig. 9. Calibration curve for the H_{α}/O ratio obtained by the averaging and the instantaneous methods.

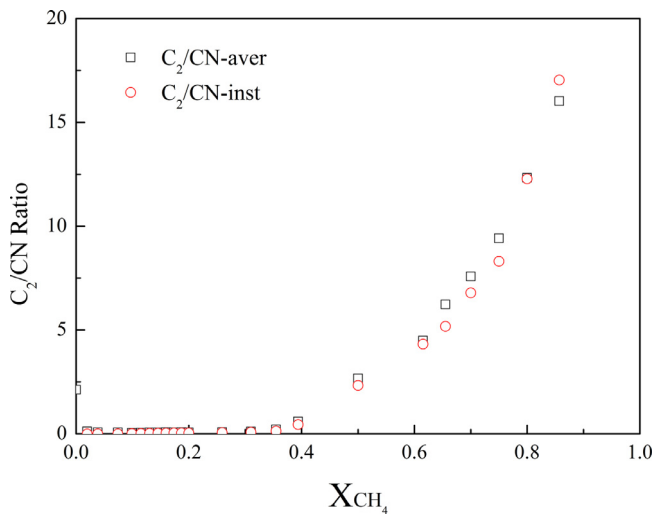


Fig. 10. Calibration curve for the C_2/CN ratio obtained by the averaging and the instantaneous methods.

[24,25] and Joshi et al. [20], where shot-to-shot measurements were carried out in different combustion systems. Initially, Ferioli et al. performed LIBS experiments in a four-cylinder engine [25] and later in a 25-mm-ID burner. Similarly to our strategy, two different ways were used for the analysis of the results during the experiments in the engine system [25] that had overall lean mixtures. The relative standard deviation in their case was ranging between 2.7 and 3% of the mean value which was less than the one in the present experiments. Joshi et al. [20] managed to both ignite and measure the equivalence ratio in a variable compression single cylinder CFR engine via the single-shot methodology. The variation of the equivalence ratio, which was calculated to be less than 10%, was related primarily to the fluctuations of the overall equivalence ratio at the spark location linked to the in-cylinder mixing. Both these experiments showed a smaller rms relative to the mean than our experiments, which could be related to the collection spectrometer and delay used.

The difference between the instantaneous and the averaging approaches is shown in Figs. 9 and 10 for the H_{α}/O and C_2/CN ratios respectively for the range in which each ratio is intended to be used. Clearly, the two approaches are very close for lean (based on H_{α}/O) and for very rich compositions (based on C_2/CN). How-

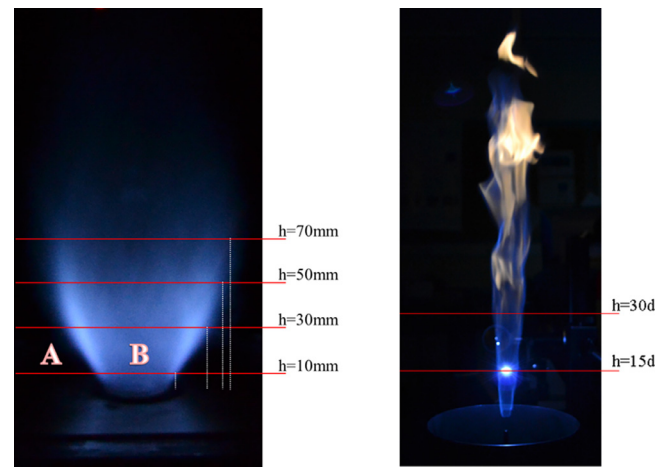


Fig. 11. Left: Photograph of the swirling premixed flame. Equivalence ratio: 0.81, velocity at annulus 10.2 m/s. Right: Photograph of the lifted methane air flame with a spark visible. Jet velocity 17 m/s, jet fluid composition 70% CH_4 , 30% air by volume. The horizontal lines on each photo reflect the locations where radial profiles of equivalence ratio were taken. Not to scale.

ever, the precision of the single-shot measurement is not good for shot-to-shot measurements in the range $0.15 < X_{CH_4} < 0.35$, where the H_{α}/O atomic lines ratio can still be used (Fig. 6a), but with the upper limit dependent on the laser energy. Alternatively, the fact that there may be significant shot-to-shot variations of the chosen ratios for some mixture compositions may put in question the averaging method used for calibration and/or measurement. This is because, if the average of each peak is first calculated by the spectrometer and then the ratio taken, this procedure is not necessarily identical to finding the ratio and then averaging.

It can be concluded that, for lean mixtures, the LIBS measurement in turbulent flames using a non-gated detector spectrometer can provide instantaneous mixture fraction measurement of acceptable precision for mixtures up to stoichiometric, but also that the error may reach about 25% of the mean for very rich mixtures.

3.3. Lean turbulent premixed flame

Figure 11a shows the swirling recirculating premixed methane-air flame studied. The equivalence ratio in this flame is expected to be constant across the reactants (region A) and the products (B), but it is expected to reduce to zero at the edges of the annular jet towards the ambient air and to decrease as we go downstream. The results of Fig. 12a, which were acquired using the instantaneous method, reproduces these expectations. In particular, the central region of the flame, which is filled with combustion products, is measured to have the same equivalence ratio as the incoming mixture, as it should. This demonstrates that the technique measures the correct ϕ in the hot products of a turbulent premixed flame.

In addition, the shot-to-shot method seems to produce more consistent results than the averaging method at the flame front, across which ϕ is again uniform, as expected (Fig. 12b). The rms of equivalence ratio in the hot products region is about 10% of the mean (not shown here), which is consistent with the shot-to-shot measurements in Section 3.2 and quantifies in an alternative way the precision of the technique. Moreover in Fig. 12b, we used two different approaches to post-process the acquired results with the instantaneous method. In both cases, we measured the intensity of each spectral line resulting in 100 different values of the intensity of H, O, C_2 and CN. In the first approach we calculated the average ratio of these 100 measurements and we derived the mean equivalence ratio; this method is called here “aver*”. In the second

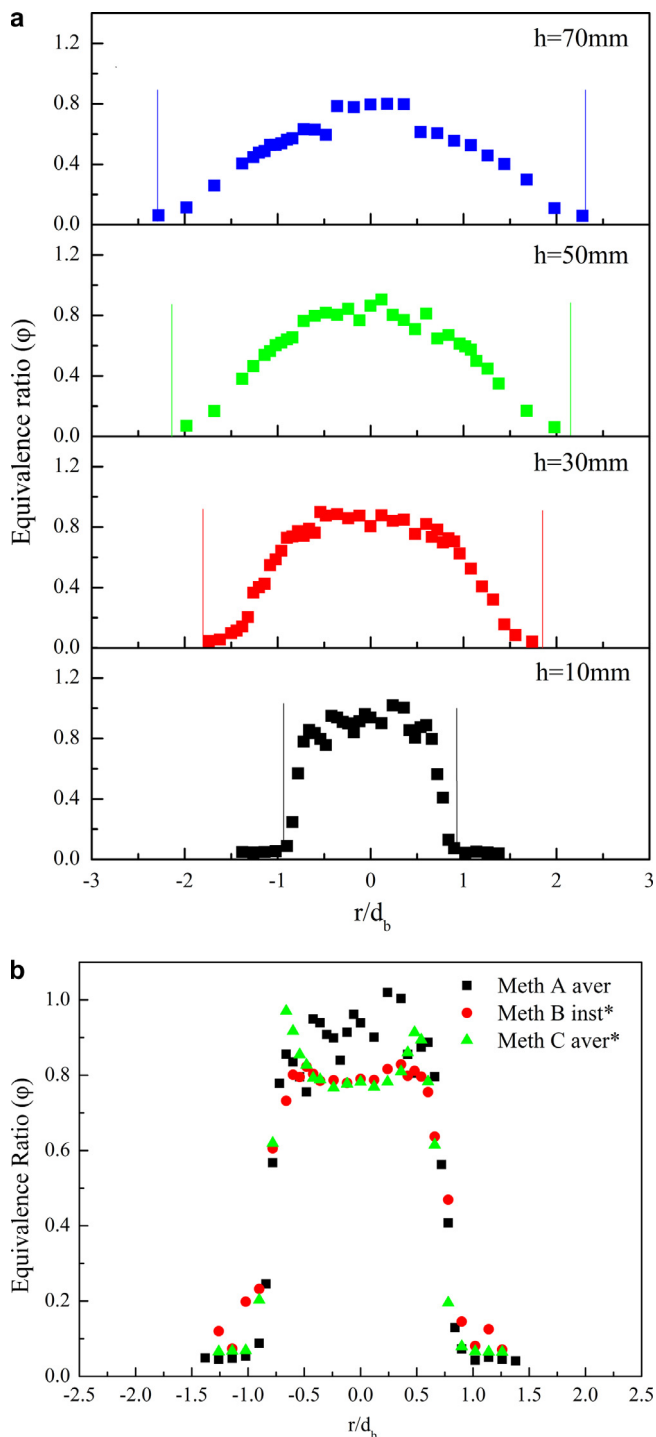


Fig. 12. (a) Radial distribution of mean ϕ in the premixed recirculating flame at different axial distances from the bluff body. (b) Radial distribution of ϕ derived from the two analytical methods of processing LIBS spectra (averaging and instantaneous).

approach, based on the 100 different ratios we calculated 100 values of the equivalence ratio, and then we averaged these 100 values of the equivalence ratio in order to get the mean; this method is called here “inst*”. Clearly, both approaches provide the mean equivalence ratio, but only the second one provides a measurement of the instantaneous equivalence ratio (or mixture fraction) from which higher statistics (e.g. the RMS) can be evaluated.

As can be seen from Fig. 12b, the method here called inst* gives better results and it has been the one used in all case where

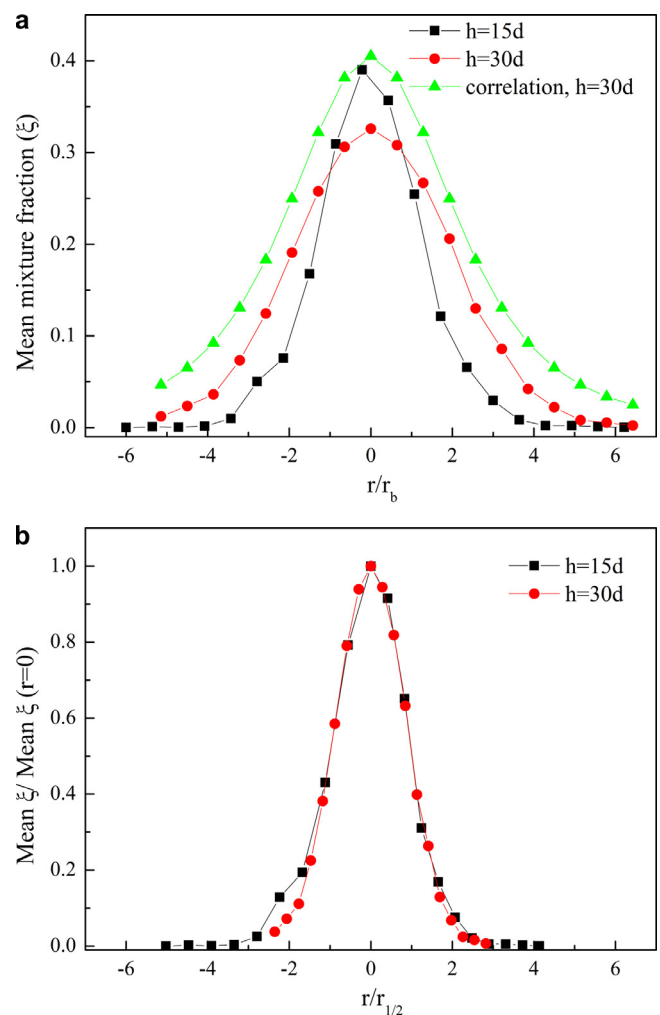


Fig. 13. (a) Distribution of mean mixture fraction (ξ) in the turbulent jet flame at two different axial stations versus the radial position (r/d). Included is the empirical fit from Lawn [47]. (b) The same data, but normalized by the centerline value plotted versus radial distance normalized by the jet half-width (i.e. the radius where the mixture fraction falls to half its centerline value).

instantaneous measurements have been performed. These results demonstrate that the spectra of the laser sparks occurring everywhere in the flame can be used for the determination of the equivalence ratio both in the reactants and the products zones of turbulent premixed flames.

3.4. Non-premixed jet flame

Figure 11b shows the lifted jet flame studied, including an indication of the axial stations where the mixture fraction measurement was performed. Note that the flame was lifted. This flame was achieved with 30% air mixed with the fuel, which is small enough premixing for the flame to be of non-premixed character. In a second series of experiments, the amount of fuel at the jet was very small (30% by volume), which does not result in an established flame and the fuel behaves like a passive tracer. However, the presence of fuel can still be detected by the LIBS spectra providing hence a measurement of the mixture fraction in a non-reacting axisymmetric jet, for which significant information exists for comparison purposes.

Figure 13 shows the mean mixture fraction (ξ), based on 100 instantaneous spectra at each point shown, for the lifted flame. Each of these spectra has been analyzed with the instantaneous

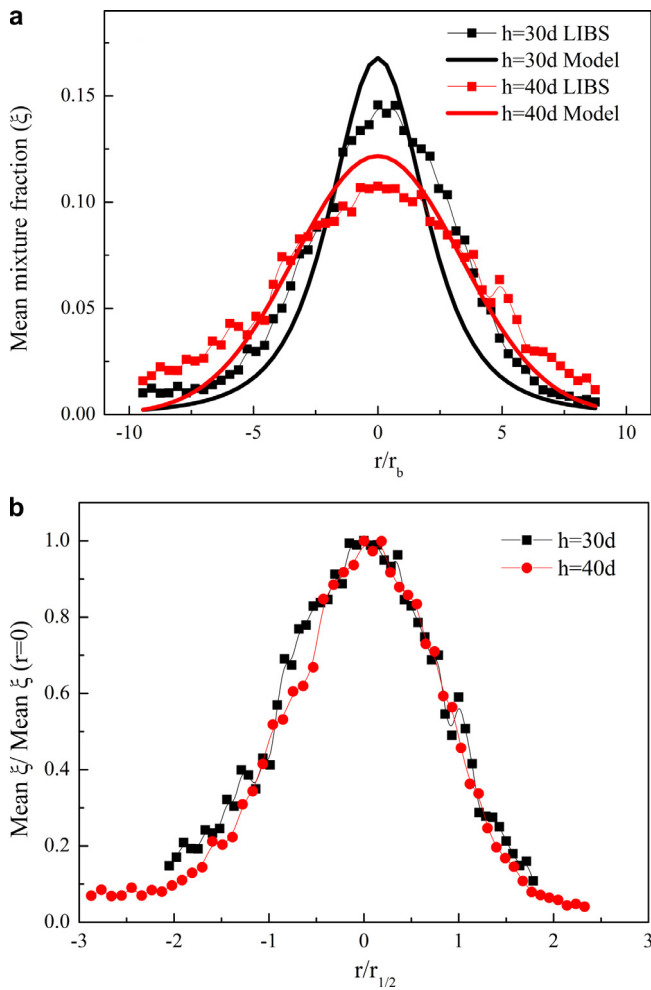


Fig. 14. (a) Radial distribution of mean mixture fraction in the non-reacting jet at two different axial stations as a function of the radial position r/d . Included is the empirical fit from Lawn [47]. (b) The same data, but normalized by the centerline value plotted versus radial distance normalized by the jet half-width.

method (described in Section 3.2). Also, the ratio H/O was used in all cases for the determination of the mixture fraction, unless the C_2 molecular band was observable in the emission spectra and the C_2/CN ratio was then used for the mixture fraction determination. Also each spectrum provided a single value of carbon mass fraction, which was further normalized by the value at the nozzle exit to give the mixture fraction. Note that the claim that the measurement gives the mixture fraction relies on the assumption that the LIBS $H\alpha/O$ and C_2/CN ratios are independent from whether the mixture is unreacted or fully burnt. This assumption is partly justified by the data with the premixed flame (Section 3.3), which gave the same equivalence ratio in the products and the reactants of a premixed flame. In the jet diffusion flame (Fig. 11b) a wide range of compositions is expected and reaction progress to be observed at the same point due to the intense inhomogeneity of the mixture and the flame base fluctuations. It is not easy to assess the quantitative accuracy of the data in Fig. 13, since an independent measurement of mixture fraction is not available. However, further exploration of the data leads to some interesting implications. First, when the mean mixture fraction (ξ) is normalized by the value at the centerline, a self-similar profile emerges (Fig. 13, right), which is according to the expectations. Second, the mixture fraction profile measured is not far from empirical correlations [47], as shown in Fig. 14. (When the jet mixing correlation is applied to flames, the burnt gases density has been used, following Ref. [48]).

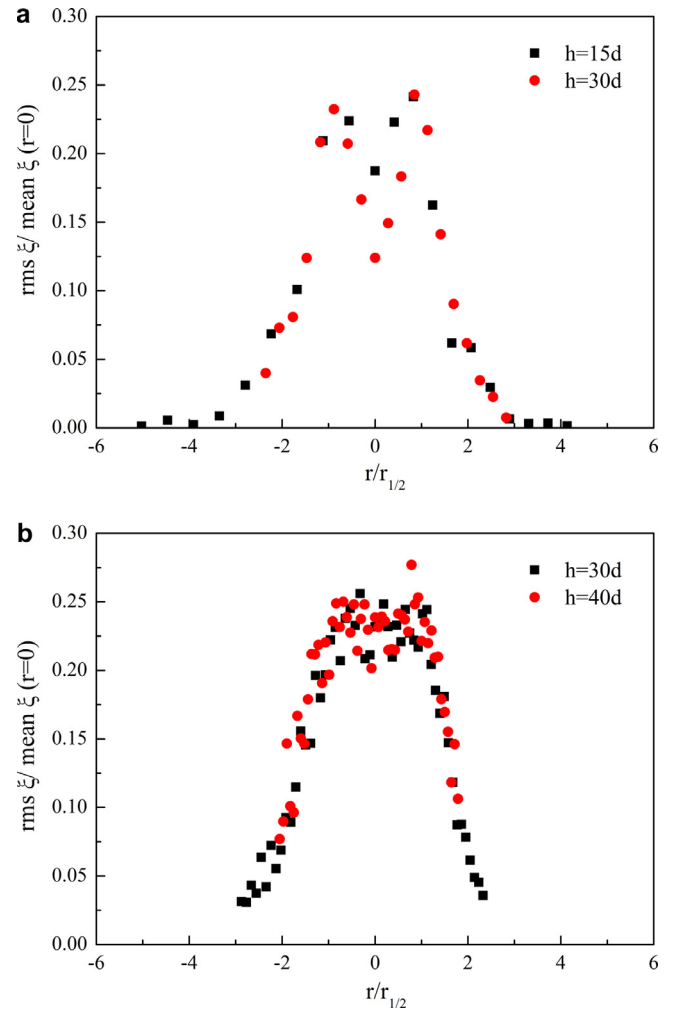


Fig. 15. Radial distribution of the rms of the mixture fraction, divided by the mean mixture fraction at the centerline at the same axial location, for the reacting (left) and non-reacting (right) jets.

In Fig. 14, similar measurements of the fuel mass fraction have been performed in a jet with low CH_4 concentration which does not lead to the establishment of a self-sustained flame. Obviously, the region hit by the laser spark temporally reacts due to the local initiation of chemical reactions, but the dominant streamwise flow takes these ignited fluid particles downstream, no flame propagates upstream, and so the parts of the jet upstream of the LIBS volume are not affected. This means that we can treat the mixing patterns before the LIBS spark as inert. It is clear from Fig. 14 that the LIBS measurement reproduces the self-similar behavior expected in inert turbulent axisymmetric jets and that the measurement are in good agreement with previous passive scalar mixing experiments [47].

The single spectra acquired here at every point resulted in a single measurement of mixture fraction, from which the mean was calculated and presented in Figs. 13 and 14. The rms values of the instantaneous mixture fraction, normalized by the measured mean value at the centerline, are shown in Fig. 15. The ratio rms/mean scalar at the centerline of turbulent axisymmetric jets in the self-preservation region reaches an asymptotic value of about 20–25% [49] and the present measurements give that this ratio is approximately constant with streamwise distance and has values in a similar range. In addition, the radial profiles are self-similar. Towards the edges of the jet, the rms smoothly decreases to zero, as expected. The non-reacting jet shows an rms that is slightly

increasing over the centerline value as we move off-axis, consistent with the expected behavior [49]. We may therefore conclude that the present LIBS system reproduces reasonably well the expected rms of the mixture fraction in this turbulent jet.

Compared to the non-reacting jet, the reacting jet has lower mixture fraction fluctuations and there is a more pronounced increase off-axis, with the peak occurring at a radius equal to the jet's half-width. These trends are consistent with the measurements in the Sandia piloted jet flames [50], where the rms over the mean at the centerline was about 0.1–0.13, and the peak normalized rms reached values of about 0.2–0.25. Note that the reasonable measurement of the rms shown here is mostly attributed to the fact that in the present experiments the absolute amount of fuel is low at the measurement locations due to mixing with ambient air and due to the air premixing in the jet fluid, which means there are very few samples with large enough carbon content to give C_2 signal and hence rely on the C_2/CN part of the calibration scheme that has lower precision.

These results and the good agreement with the expected mixture fraction distribution in jets suggests that the present LIBS technique, with the novel calibration scheme proposed, can measure the mean mixture fraction (ξ) in turbulent non-premixed systems with acceptable accuracy. It can also provide a good approximation to the rms of the mixture fraction, provided there are not too many fluid samples with very high carbon content. For very rich locations, we may expect that the mean is captured well, but that the rms is measured higher than the true rms due to the lower precision or higher uncertainty associated with the generation of the C_2 lines.

4. Conclusions

Exploration of the Laser-Induced Breakdown Spectroscopy technique for uniform methane–air mixtures spanning a wide range of compositions and for turbulent non-premixed and premixed flames has been performed. The differences among the various spectra are discussed and the intensity ratios $H_\alpha(656.3\text{ nm})/O(777.3\text{ nm})$ and $C_2(516.5\text{ nm})/CN(388.3\text{ nm})$ were found to depend monotonically and almost linearly to the mole fraction of methane in the ranges 0–0.3 and of 0.3–1.0 respectively, therefore providing a novel scheme for measurement in non-premixed systems spanning a wide range of equivalence ratios. It is found that, with proper attention to the calibration and to the laser energy, the local equivalence ratio in flames can be measured from both unreacted and reacted mixtures, in both premixed and non-premixed flames, and in inert mixing flows. The spectrometer with the non-gated detector used here allows simpler and low-cost measurements in various combustion systems with reasonable accuracy.

Acknowledgments

At Patras, this research has been co-financed by the European Union (European Social Fund – ESF) and Greek national funds through the Operational Program "Education and Lifelong Learning" of the National Strategic Reference Framework (NSRF) – Research Funding Program: Heracleitus II. Investing in knowledge society through the European Social Fund. MK acknowledges the Heracleitus II Program for a Ph.D fellowship and ERASMUS placement program that made possible a visit to the University of Cambridge in 2013. At Cambridge, RY has been funded by the Dorothy Hodgkin studentship program of the EPSRC.

References

- [1] W. Miziolek, V. Palleschi, I. Schechter, Laser induced breakdown spectroscopy (LIBS): fundamentals and applications, Cambridge University Press, New York, 2006, Chapter 5.
- [2] R. Noll, Laser-induced breakdown spectroscopy fundamentals and applications, Elsevier, Verlag, Berlin, Heidelberg, 2012 Chapter 14.6.
- [3] J.P. Singh, S.N. Thakur, Laser induced breakdown spectroscopy, Elsevier, Amsterdam, The Netherlands, 2007, Chapter 9.
- [4] T.X. Phuoc, F.P. White, Laser induced spark for measurements of the fuel-to-air ratio of a combustible mixture, *Fuel* 81 (2002) 1761–1765.
- [5] T.-W. Lee, N. Hegde, Laser-induced breakdown spectroscopy for in situ diagnostics of combustion parameters including temperature, *Combust. Flame* 142 (2005) 314–316.
- [6] A. Michalakou, P. Stavropoulos, S. Couris, Laser-induced breakdown spectroscopy in reactive flows of hydrocarbon-air mixtures, *Appl. Phys. Lett.* 92 (2008) 081501–1–3.
- [7] R.W. Schmieder, Combustion applications of laser-induced breakdown spectroscopy, *Electro-Optics Laser Conference*, Cahners, Chicago, IL (1981), p. 17.
- [8] J. Kiefer, J.W. Troger, Z. Li, T. Seeger, M. Alden, A. Leipertz, Laser-induced breakdown flame thermometry, *Combust. Flame* 159 (2012) 3576–3582.
- [9] J. Kiefer, Z. Li, M. Alden, Laser-induced breakdown spectroscopy in a partially premixed turbulent jet flame, *Meas. Sci. Technol.* 24 (2013) 075205 1–6.
- [10] J. Kiefer, J.W. Tröger, Z.S. Li, M. Alden, Laser-induced plasma in methane and dimethyl ether for flame ignition and combustion diagnostics, *Appl. Phys. B* 103 (2011) 229–236.
- [11] P. Stavropoulos, A. Michalakou, G. Skevis, S. Couris, Quantitative local equivalence ratio determination in laminar premixed methane–air flames by laser induced breakdown spectroscopy (LIBS), *Chem. Phys. Lett.* 404 (2005) 309–314.
- [12] P. Stavropoulos, A. Michalakou, G. Skevis, S. Couris, Laser-induced breakdown spectroscopy as an analytical tool for equivalence ratio measurement in methane–air premixed flames, *Spectrochim. Acta B* 60 (2005) 1092–1097.
- [13] A.E. Majd, A.S. Arabanian, R. Massudi, M. Nazeri, Spatially resolved laser-induced breakdown spectroscopy in methane–air diffusion flames, *Appl. Spectrosc.* 65 (1) (2011) 36–42.
- [14] T.X. Phuoc, Laser-induced spark for simultaneous ignition and fuel-to-air ratio measurements, *Opt. Laser Eng.* 44 (2006) 520–534.
- [15] K.E. Eseller, F.Y. Yueh, J.P. Singh, Laser-induced breakdown spectroscopy measurement in methane and biodiesel flames using an ungated detector, *Appl. Optics* 47 (31) (2008) G144–G148.
- [16] M. Buschbeck, F. Buchler, T. Halfmann, S. Arndt, Laser-induced breakdown spectroscopy for lambda quantification in a direct-injection engine, *Spectrochim. Acta B* 74–75 (2012) 103–108.
- [17] L. Zimmer, S. Tachibana, Laser induced plasma spectroscopy for local equivalence ratio measurements in an oscillating combustion environment, *Proc. Combust. Inst.* 31 (2007) 737–745.
- [18] T.X. Phuoc, R.-H. Chen, Use of laser-induced spark for studying ignition stability and unburned hydrogen escaping from laminar diluted hydrogen diffusion jet flames, *Opt. Laser Eng.* 45 (2007) 834–842.
- [19] M.S. Bak, S.-K. Im, M.G. Mungal, M.A. Cappelli, Studies on the stability limit extension of premixed and jet diffusion flames of methane, ethane, and propane using nanosecond repetitive pulsed discharge plasmas, *Combust. Flame* 160 (2013) 2396–2403.
- [20] S. Joshi, D.B. Olsen, C. Dumitrescu, V. Puzinauskas, A.P. Yalin, Laser-induced breakdown spectroscopy for in-cylinder equivalence ratio measurements in laser-ignited natural gas engines, *Appl. Spectrosc.* 63 (5) (2009) 549–554.
- [21] S. Zhang, X. Yu, F. Li, G. Kang, L. Chen, Z. Zhang, Laser induced breakdown spectroscopy for local equivalence ratio measurement of kerosene/air mixture at elevated pressure, *Opt. Laser Eng.* 50 (2012) 877–882.
- [22] M.M. Tripathi, K.K. Srinivasan, S.R. Krishnan, F.-Y. Yueh, J.P. Singh, A comparison of multivariate LIBS and chemiluminescence-based local equivalence ratio measurements in premixed atmospheric methane–air flames, *Fuel* 106 (2013) 318–327.
- [23] L. Zimmer, S. Yoshida, Feasibility of laser-induced plasma spectroscopy for measurements of equivalence ratio in high-pressure conditions, *Exp. Fluids* 52 (4) (2012) 891–904.
- [24] F. Ferioli, S.G. Buckley, Measurements of hydrocarbons using laser-induced breakdown spectroscopy, *Combust. Flame* 144 (2006) 435–447.
- [25] F. Ferioli, P.V. Puzinauskas, S.G. Buckley, Laser-Induced Breakdown Spectroscopy for On-Line Engine Equivalence Ratio Measurements, *Appl. Spectrosc.* 57 (9) (2003) 1183–1189.
- [26] C. Letty, A. Pastore, E. Mastorakos, R. Balachandran, S. Couris, Comparison of electrical and laser spark emission spectroscopy for fuel concentration measurements, *Exp. Therm. Fluid Sci.* 34 (2010) 338–345.
- [27] M. Kotzagianni, S. Couris, Femtosecond laser induced breakdown for combustion diagnostics, *Appl. Phys. Lett.* 100 (2012) 264104 1–4.
- [28] M. Kotzagianni, S. Couris, Femtosecond laser induced breakdown spectroscopy of air–methane mixtures, *Chem. Phys. Lett.* 561–562 (2013) 36–41.
- [29] H. Do, C. Carter, Hydrocarbon fuel concentration measurement in reacting flows using short-gated emission spectra of laser induced plasma, *Combust. Flame* 160 (2013) 601–609.
- [30] M. Kotzagianni PhD thesis, In situ, fast and non-perturbative diagnostics of combustion processes and its products using laser induced breakdown spectroscopy (LIBS), University of Patras, Greece, 2014.

- [31] S.F. Ahmed, E. Mastorakos, Spark ignition of lifted turbulent jet flames, *Combust. Flame* 146 (2006) 215–231.
- [32] D.E. Cavaliere, J. Kariuki, E. Mastorakos, A comparison of the blow-off behaviour of swirl-stabilized premixed, non-premixed and spray flames, *Flow Turbul. Combust.* 91 (2) (2013) 347–372.
- [33] L. Zimmer, K. Okai, Y. Kurosawa, Combined laser induced ignition and plasma spectroscopy: fundamentals and application to a hydrogen-air combustor, *Spectrochim. Acta B* 62 (12) (2007) 1484–1495.
- [34] G.M. Fuge, M.N.R. Ashfold, S.J. Henley, Studies of the plume emission during the femtosecond and nanosecond ablation of graphite in nitrogen, *J. Appl. Phys.* 99 (1) (2006) 014309 1–12.
- [35] H.S. Park, S.H. Nam, S.M. Park, Time-resolved optical emission studies on the laser ablation of a graphite target: the effects of ambient gases, *J. Appl. Phys.* 97 (11) (2005) 113103 1–5.
- [36] A. Kido, K. Hoshi, H. Kusaka, H. Ogawa, N. Miyamoto, Instantaneous measurement of local concentration and vapor fraction in liquid-gas mixtures by laser-induced breakdown spectroscopy, *JSME Int. J. B-Fluid T* 49 (2) (2006) 520–525.
- [37] V. Sturm, R. Noll, Laser-induced breakdown spectroscopy of gas mixtures of air, CO₂, N₂, and C₃H₈ for simultaneous C, H, O, and N measurement, *Appl. Optics* 42 (30) (2003) 6221–6225.
- [38] H.-L. Li, H.-L. Xu., B.-S. Yang, Q.-D. Chen, T. Zhang, H.-B. Sun, Sensing combustion intermediates by femtosecond filament excitation, *Opt. Lett.* 38 (8) (2013) 1250–1252.
- [39] T. Agarwal, F. Richecoeur, L. Zimmer, Application of two dimensional laser induced plasma spectroscopy to the measurement of local composition in gaseous flows, 15th Int Symp on Applications of Laser Techniques to Fluid Mechanics, Lisbon, Portugal, 05–08 July (2010).
- [40] H. Huang, L.M. Yang, J. Liu, Qualitative assessment of laser-induced breakdown spectra generated with a femtosecond fiber laser, *Appl. Opt.* 51 (36) (2012) 8669–8676.
- [41] J. Goujon, A. Giakoumaki, V. Piñon, O. Musset, D. Anglos, E. Georgiou, J.P. Boquillon, A compact and portable laser-induced breakdown spectroscopy instrument for single and double pulse applications, *Spectrochim. Acta B* 63 (2008) 1091–1096.
- [42] H. Heilbrunner, N. Huber, H. Wolfmeir, E. Arenholz, J.D. Pedarnig, J. Heitz, Comparison of gated and non-gated detectors for double-pulse laser induced plasma analysis of trace elements in iron oxide, *Spectrochim. Acta B* 74–75 (2012) 51–56.
- [43] M. Mueller, I.B. Gornushkin, S. Florek, D. Mory, U. Panne, Approach to detection in laser-induced breakdown spectroscopy, *Anal. Chem.* 79 (2007) 4419–4426.
- [44] P. Robert, C. Fabre, J. Dubessy, M. Flin, M.C. Boiron, Optimization of micro-Laser Induced Breakdown Spectroscopy analysis and signal processing, *Spectrochim. Acta B* 63 (2008) 1109–1116.
- [45] A. Giakoumaki, I. Osticioli, D. Anglos, Spectroscopic analysis using a hybrid LIB-S-Raman system, *Appl. Phys. A* 83 (2006) 537–541.
- [46] A.P.M. Michel, Review: Applications of single-shot laser-induced breakdown spectroscopy, *Spectrochim. Acta B* 65 (2010) 185–191.
- [47] C.J. Lawn, Lifted flames on fuel jets in co-flowing air, *Prog. Energ. Combust.* 35 (2009) 1–30.
- [48] R.W. Bilger, A mixture fraction framework for the theory and modeling of droplets and sprays, *Combust. Flame* 158 (2011) 191–202.
- [49] C.D. Richards, W.M. Pitts, Global density effects on the self-preservation behaviour of turbulent free jets, *J. Fluid Mech.* 254 (1993) 417–435.
- [50] J.H. Frank, R.S. Barlow, C. Lundquist, Radiation and nitric oxide formation in turbulent non-premixed jet flames, *Proc. Combust. Inst.* 28 (2000) 447–454.